Millimeter-Wave Downlink Positioning with a Single-Antenna Receiver

Citation for the original published paper (version of record):
Fascista, A., Coluccia, A., Wymeersch, H. et al (2019). Millimeter-Wave Downlink Positioning with a Single-Antenna Receiver. IEEE Transactions on Wireless Communications, early access(9): 4479-4490. http://dx.doi.org/10.1109/TWC.2019.2925618

(article starts on next page)

Millimeter-Wave Downlink Positioning with a Single-Antenna Receiver

Alessio Fascista, *Student Member, IEEE*, Angelo Coluccia, *Senior Member, IEEE*, Henk Wymeersch, *Member, IEEE*, and Gonzalo Seco-Granados, *Senior Member, IEEE*

***Abstract*—The paper addresses the problem of determining the unknown position of a mobile station for a mmWave MISO system. This setup is motivated by the fact that massive arrays will be initially implemented only on 5G base stations, likely leaving mobile stations with one antenna. The maximum likelihood solution to this problem is devised based on the time of flight and angle of departure of received downlink signals. While positioning in the uplink would rely on angle of arrival, it presents scalability limitations that are avoided in the downlink. To circumvent the multidimensional optimization of the optimal joint estimator, we propose two novel approaches amenable to practical implementation thanks to their reduced complexity. A thorough analysis, which includes the derivation of relevant Cramér-Rao lower bounds, shows that it is possible to achieve quasi-optimal performance even in presence of few transmissions, low SNRs, and multipath propagation effects.**

***Index Terms*—mmWave, positioning, massive MIMO, MISO, 5G cellular networks, angle of departure (AOD), beamforming**

I. Introduction

MILLIMETER-WAVE (mmWave) and massive multiple-input multiple-output (MIMO) technologies are currently regarded as strong candidates for next-generation wireless systems, including vehicular and 5G cellular networks. Indeed, such technologies not only are key enabler of high data rates and spectral efficiency [1]–[5], but also they are promising tools for precise localization thanks to their high temporal resolution and high directivity [6]–[10].

The theoretical localization performance achievable using mmWave MIMO have been recently investigated in [11]–[13]. In [13], the Cramér-Rao Lower bound (CRLB) on the position and rotation angle estimates obtained using mmWave from a single transmitter has been derived. Furthermore, a novel position and rotation estimation algorithm based on compressed sensing that attains the CRLB for average to high signal-to-noise ratio (SNR) is proposed. In [11], fundamental limits of position and orientation estimation for uplink and downlink in 3D-space were presented. Authors in [12] have shown that non-line-of-sight (NLOS) components can also be exploited to gain additional information for position and orientation estimation.

A few papers have proposed more sophisticated localization schemes, trying to take advantage of the peculiarities of mmWave and (massive) MIMO technologies. In [14], a 3D indoor positioning scheme based on hybrid received signal strength (RSS) and Angle-Of-Arrival (AOA), which employs only a single base station (BS) has been presented. A hypothesis testing localization approach is proposed in [15] exploiting the concept of channel sparsity. A low-complexity AOA-based approach with signal subspace reconstruction is devised in [16] to localize incoherently distributed sources. An extended Kalman filter (EKF) tracking algorithm that jointly exploits AOA and time of flight (TOF) from uplink reference signals has been proposed in [17]. In [18], a direct position estimation algorithm is derived. It is based on a compressed sensing framework that exploits some channel properties to identify NLOS signal paths, leading to superior performance compared to other approaches. Authors in [19] addressed the problem of positioning based on joint TOF, Angle-of-Departure (AOD), and AOA estimation and investigated the impact of errors in delays and phase shifters. A hybrid time-difference-of-arrival (TDOA), AOA, and AOD localization scheme is presented in [20] based on linearization of a set of local constraints, while in [21] positioning is addressed using a Gaussian process regressor based on a fingerprinting technique operating on a vector of RSS measurements.

It is worth noticing that almost all the aforementioned approaches heavily rely on the adoption of (possibly large) multi-antenna systems at both transmitter and receiver sides. Although this setup allows for efficient channel estimation by employing high directional beamforming to compensate severe path loss [22], it requires that commercial massive MIMO implementations for mobile stations (MSs) (e.g., smartphones) will be available in the very near term [23]. However, as recent research showed, it is reasonable to expect that MSs will likely have one (or very few) antennas, while massive arrays will be initially implemented only at the BSs side [24], [25].

In this work, we address the problem of estimating the unknown MS position under a multiple-input single-output (MISO) system setup. The processing is done exclusively on-board at the MS by exploiting the known signals transmitted by a single BS, without any increase in the bandwidth consumption, and requiring an antenna array only on the BS (as opposed to MIMO scenarios). While conventional localization schemes that exploit angular information mainly

This work was supported in part by the EU-H2020 project 5GCAR (Fifth Generation Communication Automotive Research and innovation), and in part by the Research and Development Projects of Spanish Ministry of Science, Innovation and Universities TEC2017-89925-R and TEC2017-90808-REDT.

A. Fascista and A. Coluccia are with the Department of Innovation Engineering, Università del Salento, Via Monteroni, 73100 Lecce, Italy (e-mail: alessio.fascista@unisalento.it; angelo.coluccia@unisalento.it).

G. Seco-Granados is with the Department of Telecommunications and Systems Engineering, Universitat Autònoma de Barcelona, 08193 Barcelona, Spain (e-mail: gonzalo.seco@uab.cat).

H. Wymeersch is with the Department of Electrical Engineering, Chalmers University of Technology, 412 96 Gothenburg, Sweden (e-mail: henkw@chalmers.se).

focus on AOA estimation, the proposed approach uses the AOD of received downlink signals. The underlying idea in the estimation of the AOD with a single antenna receiver is the exploitation of the fact that the different transmitted beams are received with different amplitude (magnitude and phase) depending on the direction on which the receiver is seen from the transmitter. If a single beam is transmitted, the estimation of the AOD is not possible because the received signal amplitude depends on the beam pattern but also on the unknown channel amplitude. Conversely, when more beams are transmitted, AOD estimation is possible because the ratio between the received amplitudes from different beams depends on the beam patterns, not on the channel gain, and hence on the direction from which the MS is reached. Note that the beams with different spatial patterns (obtained by precoding through the beamforming matrix) can be transmitted exploiting the different degrees of diversity in the system. That is, beams can be transmitted sequentially (time division), or at different subcarriers (frequency division). Our results also indicate that in the mmWave MISO setup accurate positioning is possible even using a single omnidirectional antenna at the MS, a foreseen scenario for the very near future, before full-fledged MIMO technologies will be available. This approach has several advantages.

First of all, the uplink channel is used only for preliminary synchronization of the receiver; then, several subsequent position estimate updates can be performed by exploiting the sole downlink channel (instead of performing AOA estimation at the BS side using the uplink channel). In doing so, there is an important saving of uplink bandwidth and energy on the MS, which is known to be much more resource-constrained compared to BSs. It is worth highlighting that future 5G networks envision the presence of a massive number of *low-power* devices (in addition to smartphones) that need to transmit data to the BS under the internet-of-things (IoT) paradigm, which is expected to overload the uplink (medium access) channel; at the same time, position estimates need to be provided at high rate in some emerging applications that are driving the 5G revolution (e.g., for safety). In such a scenario, thus, saving energy and uplink resources while achieving high-rate positioning is of key importance. An additional advantage of performing downlink positioning on MSs is that it distributes the localization task, thus avoiding the BS to take such a burden for all terminals (as conversely required by uplink positioning), especially because the number of connected devices is exponentially growing, as mentioned. In other words, downlink positioning allows multiple (potentially unlimited) terminals to be localized by opportunistically exploiting a single transmission from the BS (e.g., a broadcast control channel) with no overhead for the system.

The paper provides two kinds of contributions. First, we thoroughly analyze the problem from a theoretical perspective, deriving the exact solution to the Maximum Likelihood (ML) estimation problem and complementing the CRLB-analysis available in the literature [11] with a precise assessment of the achievable performance under the considered MISO setup. As a second contribution, we design two novel and practical estimators with reduced complexity. In particular:

- a first estimator based on an unstructured transformation of the likelihood function is proposed, which provides an approximate solution to the exact ML problem while avoiding the burden of multidimensional optimization methods;
- a second estimation approach based on the method of moments is devised for the case of sufficient amount of received data, which results in a closed-form estimator of the TOF and hence further reduces the complexity to a single one-dimensional search.

While unstructured approximations have been proposed in the literature for joint AOA and delay estimation [26]–[28], to the best of our knowledge this is the first work in which such an approach is applied to joint AOD and delay estimation. The numerical analysis, carried out by simulating the characteristics of mmWave wireless channels, demonstrates that the proposed estimators can achieve almost the same performance of the exact ML estimator and are able to cope with the different operating conditions at play in typical mmWave channels.

It is worth highlighting that in the MISO setup addressed in this paper, unlike the MIMO case, the LOS must be present to make the localization problem solvable. Indeed, in mmWave MIMO systems all the NLOS paths can be separately estimated and exploited for localization [12], [13], while this is not possible in our setup since the MS has only one antenna. However, it should be emphasized that LOS propagation is the typical assumed scenario for mmWave communications, since the latter can unleash their potential of high directivity and high temporal resolution only in presence of a LOS path. Indeed, mmWave links are highly susceptible to blockages, even caused by the human body itself, as opposed to lower frequencies [29]. As part of an effort to overcome such issues, the mmWave research community is recently steering towards the concept of *multi-connectivity* [30]–[32]. Basically, this feature allows a MS to maintain multiple possible LOS paths to different BSs so that drops in one link can be overcome by switching data paths. Since the goal of this paper is to investigate the potential benefits of exploiting the peculiar characteristics of mmWave downlink signals, we assume the MS is operating in environments where at least one LOS path to a (non-obstructed) BS is present; in this respect, multi-connectivity provides a further justification. However, to evaluate how the performance degrade in presence of NLOS propagation (but still assuming a direct LOS path is present), in Sec. V-C we will investigate also scenarios where NLOS paths are present; we anticipate that these results show that the proposed algorithms are still effective.

The remaining of the paper is organized as follows. In Sec. II we introduce the system model and describe the reference scenario. In Sec. III we formulate the ML estimation problem and illustrate in details the design and derivation of the proposed low-complexity estimators. Then, in Sec. IV, we derive the fundamental lower bounds on the estimation uncertainty under the considered MISO setup. In Sec. V we analyze the performance, also in comparison with the uplink channel, by means of Monte Carlo simulations in different realistic scenarios. We conclude the paper in Sec. VI.

II. System Model

We consider, as a reference scenario, a MISO system with a BS equipped with N_{BS} antennas and a MS equipped with a single antenna operating at a carrier frequency f_c (corresponding to wavelength λ_c) and bandwidth B. Without loss of generality, the location of the BS is taken in the origin, while we denote by $\boldsymbol{p} = [p_x \ p_y]^{\text{T}}$ the unknown MS position.

A. Transmitter Model

We consider the transmission of orthogonal frequency division multiplexing (OFDM) signals, where the BS, implementing a hybrid analog/digital precoder at the transmitting side, communicates with the MS. Particularly, we assume that G signals are transmitted sequentially, where the g-th transmission comprises M simultaneously transmitted symbols[1] for each subcarrier $n = 0, \dots, N-1$, i.e.,

$$\boldsymbol{x}^g[n] = [x_1[n] \ \cdots \ x_M[n]]^{\text{T}} \in \mathbb{C}^{M\times 1} \quad n = 0, \dots, N-1, \tag{1}$$

and $P_t = \mathbb{E}\left[\|\boldsymbol{x}^g[n]\|^2\right]$ the transmitted power with $\mathbb{E}[\cdot]$ denoting the expectation operator. The symbols are first precoded and then transformed to the time-domain using N-point Inverse Fast Fourier Transform (IFFT). A cyclic prefix (CP) of length $T_{\text{CP}} = DT_s$ is added before applying the radio-frequency (RF) precoding, where D is the length of CP in symbols and $T_s = 1/B$ denotes the sampling period. Hereafter, we assume that T_{CP} exceeds the delay spread of the channel.

The transmitted signal over subcarrier n at time g can be expressed as $\boldsymbol{F}^g[n]\boldsymbol{x}^g[n]$, with $\boldsymbol{F}^g[n] \in \mathbb{C}^{N_{\text{BS}}\times M}$ denoting the beamforming matrix applied at the transmitting side. To lower the hardware complexity, in this work we adopt a hybrid beamforming architecture. In particular, assuming that $M_{\text{BS}}^{\text{RF}}$ RF chains are available at the BS, the beamforming matrix $\boldsymbol{F}^g[n]$ can be expressed as

$$\boldsymbol{F}^g[n] = \boldsymbol{F}_{\text{RF}}\boldsymbol{F}_{\text{BB}}^g[n] \tag{2}$$

where $\boldsymbol{F}_{\text{RF}} \in \mathbb{C}^{N_{\text{BS}}\times M_{\text{BS}}^{\text{RF}}}$ is implemented using analog phase shifters with entries of the form $\mathrm{e}^{j\phi_{m,n}}$, where $\{\phi_{m,n}\}$ are given phases, and $\boldsymbol{F}_{\text{BB}}^g[n] \in \mathbb{C}^{M_{\text{BS}}^{\text{RF}}\times M}$ is the digital beamformer. Furthermore, we impose a total power constraint $\|\boldsymbol{F}_{\text{RF}}\boldsymbol{F}_{\text{BB}}^g[n]\|_{\text{F}} = 1$ [33]. Considering the angular sparsity of the mmWave channels, one usually needs less beams than antenna elements, i.e., $M \leq N_{\text{BS}}$ [34], [35]. It should be noticed that our work does not assume any specific choice of the beamformer matrices, hence in principle any possible value for $\boldsymbol{F}^g[n]$ can be considered. Under this conservative assumption, beamformers are not required to be specifically designed for the localization task, but can simply be the same employed by the BS for communication purposes.

[1]Antenna beams employed for localization purposes should take into account the presence of users in unknown locations. For this reason, they are typically designed wide enough to cover the uncertainty region about users positions with at least two overlapping beams, irrespective of the number of antenna elements available at the BS side.

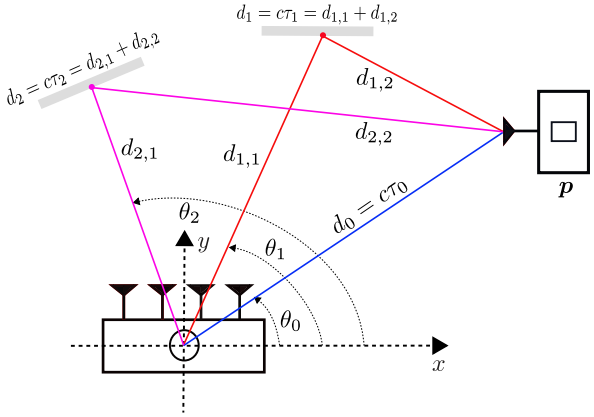

Fig. 1: Geometry of the considered scenario.

B. Channel Model

We assume that a direct Line-Of-Sight (LOS) link exists between the BS and the MS, and that additional NLOS paths due to local scatterers or reflectors may also be present. Moreover, we assume that both MS and BS are synchronized to the same clock[2]. The different position-related parameters of the channel are depicted in Fig. 1. These parameters include θ_k and τ_k, denoting the AOD and TOF related to the k-th path, respectively. In the following, $k = 0$ corresponds to the LOS link and $k > 0$ denotes the NLOS paths. Considering $K+1$ paths and a constant channel during the transmission of the G signals, the $1 \times N_{\text{BS}}$ complex channel vector associated with subcarrier n can be expressed as

$$\boldsymbol{h}^{\text{T}}[n] = \boldsymbol{\Gamma}^{\text{T}}[n]\boldsymbol{A}_{\text{BS}}^{\text{H}} \tag{3}$$

where we have exploited the fact that $\lambda_n = c/\left(\frac{n}{NT_S} + f_c\right) \approx \lambda_c \, \forall n$ (with c denoting the speed of light), i.e., the typical narrowband condition. Under this model, the array response matrix is given by

$$\boldsymbol{A}_{\text{BS}} = [\boldsymbol{a}_{\text{BS}}(\theta_0), \dots, \boldsymbol{a}_{\text{BS}}(\theta_K)] \tag{4}$$

and

$$\boldsymbol{\Gamma}[n] = \sqrt{N_{\text{BS}}} \times \begin{bmatrix} \alpha_0 \mathrm{e}^{\frac{-j2\pi n\tau_0}{NT_s}} \\ \vdots \\ \alpha_K \mathrm{e}^{\frac{-j2\pi n\tau_K}{NT_s}} \end{bmatrix} \tag{5}$$

where $\alpha_k = h_k/\sqrt{\rho_k}$, with ρ_k the path loss and h_k denoting the complex channel gain of the k-th path, respectively. The structure of the antenna steering vectors $\boldsymbol{a}_{\text{BS}}(\theta_k) \in \mathbb{C}^{N_{\text{BS}}\times 1}$ depends on the specific geometry of the considered array. Without loss of generality, in the following we consider a Uniform Linear Array (ULA) without mutual antenna coupling

[2]We rely on the commonly used synchronization assumption e.g., [8], [36]–[38], which is customary for the sake of decoupling the effect of delay estimation errors from other sources of time-related performance degradation. We recognize that in practice synchronization errors must be taken into account. This can be done by assuming that a preliminary synchronization step has been performed using, e.g., a two-way synchronization protocol [39], [40].

and with isotropic antennas, whose steering vector can be expressed as

$$\boldsymbol{a}_{\text{BS}}(\theta) = \frac{1}{\sqrt{N_{\text{BS}}}} \left[1 \; e^{j\frac{2\pi}{\lambda_c} d \sin\theta} \cdots \; e^{j(N_{\text{BS}}-1)\frac{2\pi}{\lambda_c} d \sin\theta}\right]^{\text{T}} \quad (6)$$

where $d = \frac{\lambda_c}{2}$ denotes the ULA interelement spacing.

C. Received Signal Model

The received signal related to the n-th subcarrier and transmission g, after CP removal and Fast Fourier Transform (FFT), is given by

$$y^g[n] = \boldsymbol{h}^{\text{T}}[n]\boldsymbol{F}^g[n]\boldsymbol{x}^g[n] + \nu^g[n] \quad (7)$$

where $\nu^g[n]$ is the additive circularly complex Gaussian noise with zero mean and variance σ^2. The ultimate goal of this work is to estimate the unknown MS position $\boldsymbol{p}$ from the set of all received signals

$$\boldsymbol{Y} = \begin{bmatrix} y^1[0] & \cdots & y^G[0] \\ \vdots & \ddots & \vdots \\ y^1[N-1] & \cdots & y^G[N-1] \end{bmatrix}. \quad (8)$$

To this aim, we focus on the estimation of the LOS position-related parameters θ_0 and τ_0. Based on such estimates, the unknown MS position $\boldsymbol{p}$ can be determined by recalling that the TOF defines a circle centered in the BS and with radius $d_0 = c\tau_0$ from the MS, according to

$$p_x^2 + p_y^2 = d_0^2 \quad (9)$$

while the AOD is related to the unknown MS position as

$$\theta_0 = \text{atan2}(p_y, p_x) \quad (10)$$

where the function $\text{atan2}(y, x)$ is the four-quadrant inverse tangent. Solving (9)–(10) and replacing the actual values with the estimated ones readily provides an estimate of the MS position according to

$$\hat{\boldsymbol{p}} = \hat{d}_0 \left[\cos\hat{\theta}_0 \;\; \sin\hat{\theta}_0\right]^{\text{T}}. \quad (11)$$

Fundamental lower bounds on the estimation uncertainty will be derived to evaluate the performance.

III. Angle of Departure (AOD) and Time Of Flight (TOF) Estimation

In this section, we derive novel algorithms for the estimation of the LOS channel parameters θ_0 and τ_0 in presence of the nuisance parameters α_0 and σ^2.

A. Joint Maximum Likelihood Estimation

To formulate the estimation problem, we exploit the fact that, under typical mmWave assumptions, all the paths are resolvable in either the time or space domains, and the multipath components are likely uncorrelated with the LOS [11]. Since we are interested in estimating the sole LOS position-related parameters[3], NLOS paths can be omitted from (3) and the multipath parameter estimation can be then reduced to a problem of single-path estimation, that is, the channel vector given in (3) can be re-defined as

$$\boldsymbol{h}^{\text{T}}[n] = \sqrt{N_{\text{BS}}}\alpha \, \text{e}^{\frac{-j2\pi n\tau}{NT_S}} \boldsymbol{a}_{\text{BS}}^H(\theta) \quad (12)$$

where only LOS path is considered from now on. To ease the notation, we introduce $\alpha \overset{\text{def}}{=} \alpha_0$, $\tau \overset{\text{def}}{=} \tau_0$, and $\theta \overset{\text{def}}{=} \theta_0$. Consequently, each received signal $y^g[n]$, $1 \le g \le G$, $0 \le n \le N-1$, can be statistically characterized as

$$y^g[n] \sim \mathcal{CN}(\sqrt{N_{\text{BS}}}\alpha\bar{\boldsymbol{h}}^{\text{T}}[n]\boldsymbol{F}^g[n]\boldsymbol{x}^g[n], \sigma^2) \quad (13)$$

where $\bar{\boldsymbol{h}}^{\text{T}}[n] = \text{e}^{\frac{-j2\pi n\tau}{NT_S}} \boldsymbol{a}_{\text{BS}}^H(\theta)$ and all the parameters are treated as deterministic unknowns, except the transmitted symbols $\boldsymbol{x}^g[n]$ and the beamforming matrix $\boldsymbol{F}^g[n]$, which are assumed known to the receiver. More precisely, the whole set of unknowns in $\boldsymbol{Y}$ can be arranged as

$$\boldsymbol{\varphi} = [\theta \; \tau \; \boldsymbol{\psi}^{\text{T}}]^{\text{T}} \quad (14)$$

where θ and τ represent the sole parameters of interest, while $\boldsymbol{\psi} = [\sigma^2 \; \alpha]^{\text{T}}$ denotes the vector of nuisance parameters. The ML estimator of θ and τ is given by

$$(\hat{\theta}, \hat{\tau}) = \underset{(\theta,\tau)}{\arg\max} \left[\max_{\boldsymbol{\psi}} L(\theta, \tau, \boldsymbol{\psi})\right] \quad (15)$$

where $L(\theta, \tau, \boldsymbol{\psi}) \overset{\text{def}}{=} \log f(\boldsymbol{Y}|\theta, \tau, \boldsymbol{\psi})$ and $f(\cdot)$ denotes the probability density function of the observations $\boldsymbol{Y}$ given $\boldsymbol{\psi}$ and both θ and τ. From (15) it follows that

$$L(\theta, \tau, \boldsymbol{\psi}) = -NG\log(\pi\sigma^2) - \frac{1}{2\sigma^2}\sum_{g=1}^{G} \|\boldsymbol{y}^g - \sqrt{N_{\text{BS}}}\alpha\boldsymbol{w}^g\|^2 \quad (16)$$

where we have denoted by

$$\boldsymbol{y}^g = \begin{bmatrix} y^g[0] \\ \vdots \\ y^g[N-1] \end{bmatrix} \quad (17)$$

the g-th column of the observation matrix $\boldsymbol{Y}$, and

$$\boldsymbol{w}^g = \begin{bmatrix} \bar{\boldsymbol{h}}^{\text{T}}[0]\boldsymbol{F}^g[0]\boldsymbol{x}^g[0] \\ \vdots \\ \bar{\boldsymbol{h}}^{\text{T}}[N-1]\boldsymbol{F}^g[N-1]\boldsymbol{x}^g[N-1] \end{bmatrix}. \quad (18)$$

We start by observing that the resolution of the ML estimation problem is invariant to the knowledge of σ^2; in fact, if such a parameter were unknown, it could be estimated as $\hat{\sigma}^2 = \frac{1}{NG}\sum_{g=1}^{G} \|\boldsymbol{y}^g - \sqrt{N_{\text{BS}}}\alpha\boldsymbol{w}^g\|^2$, leading to the same value of the compressed likelihood as for known σ^2, i.e.

$$\tilde{L}(\theta, \tau, \alpha) = \sum_{g=1}^{G} \|\boldsymbol{y}^g - \sqrt{N_{\text{BS}}}\alpha\boldsymbol{w}^g\|^2 \quad (19)$$

[3]The problem of MS localization in presence of NLOS paths requires to also estimate the parameters related to the multipath propagation and hence leads to a different problem. In this work, we instead estimate the LOS parameters only, assuming that only the LOS is received in order to derive relatively simple expressions of the estimators, and subsequently evaluate the robustness of the estimator in the presence of NLOS.

where $\tilde{L}(\theta,\tau,\alpha)$ is the compressed negative log-likelihood function, and the ML estimator of θ and τ reduces to

$$(\hat{\theta},\hat{\tau}) = \underset{(\theta,\tau)}{\arg\min}\left[\min_{\alpha}\tilde{L}(\theta,\tau,\alpha)\right]. \tag{20}$$

It is a simple matter to observe that the minimization of (19) with respect to $\alpha \in \mathbb{C}$ is solved by

$$\hat{\alpha} = \frac{1}{\sqrt{N_{\text{BS}}}}\frac{\sum_{g=1}^{G}(\boldsymbol{w}^g)^{\text{H}}\boldsymbol{y}^g}{\sum_{g=1}^{G}\|\boldsymbol{w}^g\|^2}. \tag{21}$$

Substituting this maximizing value back in (19) leads to

$$\tilde{L}(\theta,\tau) = \sum_{g=1}^{G}\left\|\boldsymbol{y}^g - \left(\frac{\sum_{i=1}^{G}(\boldsymbol{w}^i(\theta,\tau))^{\text{H}}\boldsymbol{y}^i}{\sum_{i=1}^{G}\|\boldsymbol{w}^i(\theta,\tau)\|^2}\right)\boldsymbol{w}^g(\theta,\tau)\right\|^2 \tag{22}$$

where we highlight the dependency of $\boldsymbol{w}$ on both τ and θ. As it can be noticed, the function in (22) cannot be expressed in terms of any projection matrix; furthermore, it is highly non-linear in both the unknown θ and τ and does not admit a closed-form solution. A possible approach to solve the estimation problem could be based on the adoption of a numerical search algorithm[4]; more precisely, a two-dimensional grid search can be used for a direct minimization of $\tilde{L}(\theta,\tau)$. To overcome the burden of a multidimensional minimization, in the following we derive two novel suboptimal methods to estimate the TOF τ. In so doing, we can put such an estimated value back in (22) and then solve for the unknown θ in the ML problem by resorting to a simple one-dimensional search.

It is worth remarking that since our approach focuses on the estimation of LOS channel parameters, the NLOS paths are not included in the model at the design stage, hence they are never exploited to gain additional position information. Although their number is limited thanks to the sparsity of the mmWave channel, in the simulation analysis conducted in Sec. V, we will investigate the sensitivity of the proposed algorithms to multipath effects according to the LOS-to-multipath ratio (LMR), the latter defined as the ratio between the power of the LOS component and the sum of powers of the NLOS multipath components.

B. Unstructured ML-based TOF Estimation

In this subsection, we propose a novel method for the estimation of the TOF τ. For the sake of exposition, we initially consider the case of single transmission, that is, $G = 1$. Stacking the observations $y[n]$ from (7), we obtain

$$\boldsymbol{y} = \sqrt{N_{\text{BS}}}\alpha\boldsymbol{D}(\tau)\bar{\boldsymbol{X}}\boldsymbol{a}^*_{\text{BS}}(\theta) + \boldsymbol{\nu} \tag{23}$$

where

$$\boldsymbol{D}(\tau) = \begin{bmatrix} 1 & & \\ & \ddots & \\ & & \text{e}^{\frac{-j2\pi(N-1)\tau}{NT_s}} \end{bmatrix} \tag{24}$$

and

$$\bar{\boldsymbol{X}} = \begin{bmatrix} (\boldsymbol{F}[0]\boldsymbol{x}[0])^{\text{T}} \\ \vdots \\ (\boldsymbol{F}[N-1]\boldsymbol{x}[N-1])^{\text{T}} \end{bmatrix}. \tag{25}$$

To formulate the estimation problem, we make use of an unstructured model for the array steering vector instead of the one parameterized by the AOD, i.e., we introduce the generic vector $\boldsymbol{b} = \sqrt{N_{\text{BS}}}\alpha\boldsymbol{a}^*_{\text{BS}}(\theta)$. Under this model, (23) can be equivalently rewritten as

$$\boldsymbol{y} = \boldsymbol{D}(\tau)\bar{\boldsymbol{X}}\boldsymbol{b} + \boldsymbol{\nu}. \tag{26}$$

As it can be noticed, the above expression is no longer an explicit function of θ, but depends only on the TOF τ. Starting from this new model and generalizing to arbitrary values of $G \geq 1$, a ML-based estimator of τ, referred to as Unstructured ML (UML), can be derived as

$$\hat{\tau}_{\text{UML}} = \underset{\tau}{\arg\min}\left[\min_{\boldsymbol{b}}\sum_{g=1}^{G}\|\boldsymbol{y}^g - \boldsymbol{D}(\tau)\bar{\boldsymbol{X}}^g\boldsymbol{b}\|^2\right] \tag{27}$$

where $\bar{\boldsymbol{X}}^g, g = 1,\ldots,G$, are known matrices which depend on the transmitted sequences and $\boldsymbol{b} \in \mathbb{C}^{N_{\text{BS}}\times 1}$ is treated as an unknown nuisance vector. It is not difficult to show that the inner minimization of (27) is solved by

$$\hat{\boldsymbol{b}}(\tau) = \bar{\boldsymbol{X}}_G^{-1}\sum_{g=1}^{G}(\bar{\boldsymbol{X}}^g)^{\text{H}}\boldsymbol{D}^{\text{H}}(\tau)\boldsymbol{y}^g \tag{28}$$

where $\bar{\boldsymbol{X}}_G \overset{\text{def}}{=} \sum_{g=1}^{G}(\bar{\boldsymbol{X}}^g)^{\text{H}}\bar{\boldsymbol{X}}^g$ and the existence of $\bar{\boldsymbol{X}}_G^{-1}$ only requires $N \geq N_{\text{BS}}$. Substituting this maximizing value back in (27) finally yields

$$\hat{\tau}_{\text{UML}} = \underset{\tau}{\arg\min}\sum_{g=1}^{G}\|\boldsymbol{y}^g - \boldsymbol{D}(\tau)\bar{\boldsymbol{X}}^g\hat{\boldsymbol{b}}(\tau)\|^2 \tag{29}$$

which can be solved by resorting to a simple one-dimensional search over the space of τ. Putting the above estimate $\hat{\tau}_{\text{UML}}$ back in (22) and solving for the unknown θ readily provides an approximate solution to the original ML problem, but at the reduced cost of two one-dimensional searches.

C. Moment-based TOF Estimation

In this section, we further investigate the problem of estimating the unknown τ when a sufficient number of transmissions G is available. We start by observing that the elements in (7) can be equivalently re-arranged as

$$\boldsymbol{y}[n] = \left[y^1[n]\cdots y^G[n]\right]^{\text{T}} \in \mathbb{C}^{G\times 1} \tag{30}$$

$$\boldsymbol{X}[n] = \left[\boldsymbol{F}^1[n]\boldsymbol{x}^1[n]\cdots\boldsymbol{F}^G[n]\boldsymbol{x}^G[n]\right] \in \mathbb{C}^{N_{\text{BS}}\times G} \tag{31}$$

$$\boldsymbol{\nu}[n] = \left[\nu^1[n]\cdots\nu^G[n]\right]^{\text{T}} \in \mathbb{C}^{G\times 1} \;\; \forall n = 0,\ldots,N-1. \tag{32}$$

We can now express the collected observations as

$$\boldsymbol{y}[n] = \sqrt{N_{\text{BS}}}\alpha\left(\bar{\boldsymbol{h}}^{\text{T}}[n]\boldsymbol{X}[n]\right)^{\text{T}} + \boldsymbol{\nu}[n] \quad n = 0,\ldots,N-1. \tag{33}$$

[4]Iterative search algorithms like the steepest descent algorithm or the Gauss-Newton method cannot be easily applied since the objective function given in (22) exhibits several local minima.

If we assume that $G \geq N_{\text{BS}}$, the known matrices $\boldsymbol{X}[n]$ have full row-rank, so that the following transformation can be applied

$$\underbrace{\boldsymbol{y}^{\text{T}}[n]\boldsymbol{X}[n]^{+}}_{\tilde{\boldsymbol{y}}_n^{\text{T}} \in \mathbb{C}^{1\times N_{\text{BS}}}} = \sqrt{N_{\text{BS}}}\alpha\bar{\boldsymbol{h}}^{\text{T}}[n] + \underbrace{\boldsymbol{\nu}_n^{\text{T}}\boldsymbol{X}_n^{+}}_{\tilde{\boldsymbol{\nu}}_n^{\text{T}} \in \mathbb{C}^{1\times N_{\text{BS}}}} \tag{34}$$

where $\boldsymbol{X}[n]^{+} = \boldsymbol{X}[n]^{\text{H}}(\boldsymbol{X}[n]\boldsymbol{X}[n]^{\text{H}})^{-1}$ denotes the Moore-Penrose right pseudo-inverse matrix. It can be observed that these new transformed observations are ruled by

$$\tilde{\boldsymbol{y}}_n^{\text{T}} \sim \mathcal{CN}_{N_{\text{BS}}}(\sqrt{N_{\text{BS}}}\alpha\bar{\boldsymbol{h}}^{\text{T}}[n], \sigma^2\boldsymbol{C}_n) \quad n = 0, \ldots, N-1 \tag{35}$$

where $\boldsymbol{C}_n = (\boldsymbol{X}[n]^{+})^{\text{H}}\boldsymbol{X}[n]^{+}$. It is worth noting that, differently from (33), the elements of each vector $\tilde{\boldsymbol{y}}_n^{\text{T}}$ are now correlated. Starting from these new observables, we can further define

$$z_n = \tilde{\boldsymbol{y}}_n^{\text{T}}\tilde{\boldsymbol{y}}_{n+1}^{*} \quad n = 0, \ldots, N-2 \tag{36}$$

where each z_n is obtained by multiplying two consecutive $\tilde{\boldsymbol{y}}_n^{\text{T}}$, with overlap. This transformation reduces the number of available observations only by one (to $N-1$).

For the new set of data $\boldsymbol{z} = [z_0 \cdots z_{N-1}]^{\text{T}}$, by exploiting the independence of the (transformed) noise vectors, it follows (hereafter we omit the dependency on θ for simplicity)

$$\begin{aligned}\mathbb{E}[z_n] &= N_{\text{BS}}|\alpha|^2\bar{\boldsymbol{h}}^{\text{T}}[n]\bar{\boldsymbol{h}}^{*}[n+1] \\ &= N_{\text{BS}}|\alpha|^2 \text{e}^{\frac{j2\pi\tau}{NT_s}}\boldsymbol{a}_{\text{BS}}^{H}\boldsymbol{a}_{\text{BS}} = N_{\text{BS}}|\alpha|^2\text{e}^{\frac{j2\pi\tau}{NT_s}}.\end{aligned} \tag{37}$$

Remarkably, this new expression does not depend on the unknown AOD θ, but it is solely parameterized as function of the TOF τ. Therefore, one can build a method-of-moment (MM) estimator from this expression

$$\hat{\tau}_{\text{MM}} = \frac{NT_s}{2\pi}\arg\left\{\frac{1}{N-2}\sum_{n=0}^{N-2} z_n\right\} \tag{38}$$

which results in a closed-form estimator of τ. By analyzing the transformed observables z_n in (36), we can derive a useful analogy with the classical frequency estimation theory. Similarly to the Kay's method presented in [41], the approach proposed in (38) exploits a one-lag sample autocorrelation function to provide a suboptimal estimator of τ. Nonetheless, even though this method could provide good estimation performance, an additional improvement can be obtained by considering higher lags in the sample autocorrelation function, as shown in [42]. Based on this result, we derive a more general multi-lag extension of the estimator in (38) as

$$\hat{\tau}_{\text{MM}}(L) = \frac{NT_s}{2\pi q(L)}\sum_{\ell=1}^{L}\ell\arg\left\{\frac{1}{N-\ell-1}\sum_{n=0}^{N-\ell-1}\tilde{\boldsymbol{y}}_n^{\text{T}}\tilde{\boldsymbol{y}}_{n+\ell}^{*}\right\} \tag{39}$$

with $L < N$ denoting the number of different lags adopted and $q(L) = \sum_{\ell=1}^{L}\ell^2 = \frac{L(L+1)(2L+1)}{6}$. As it can be observed, this new estimator weights the argument of the sample autocorrelation function by the lag ℓ. Moreover, notice that (39) with $L = 1$ is equivalent to the one-lag estimator derived in (38). Plugging the estimate $\hat{\tau}_{\text{MM}}$ in the ML estimator (22) and solving for θ yields a novel approximate solution to the ML problem, which remarkably only requires a single one-dimensional search.

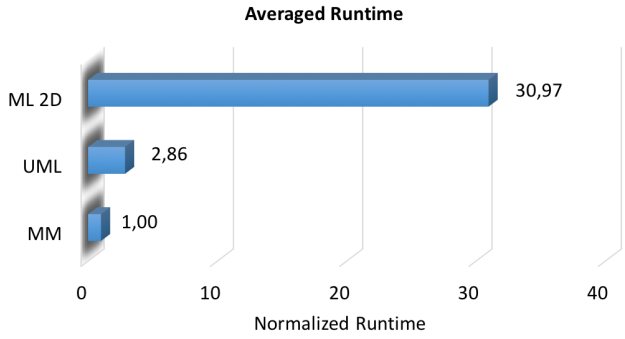

Fig. 2: Averaged runtimes of the proposed estimators.

D. Complexity Analysis

Asymptotically speaking, we observe that the complexity in performing the two-dimensional minimization in (22) is on the order of $O(P^2)$, where P denotes the number of evaluation points per dimension, while the two proposed suboptimal approaches only require $O(P)$. However, to perform a precise comparison of the actual complexity for finite values of P, we have recorded the runtimes of the estimators executed on the same hardware platform. To conduct the simulation analysis, we consider a grid of $P = 150$ evaluation points and assume $G = 10$. The average runtimes of the estimators normalized by the average runtime of the MM are given in Fig. 2. As it could be expected, the ML 2D requires by far the longest runtime due to the multidimensional search required for solving (22). On the other hand, the MM has the smallest computational complexity among all the estimators thanks to the closed-form estimation of τ performed through (39). The complexity of the UML is only about 3 times larger than that of the MM and, remarkably, is about 10 times lesser than that of the ML 2D.

To complete the analysis, we investigate the trend of the computational complexity as a function of the number of grid points P. Fig. 3 shows the average runtimes for four different values of P, normalized by the average runtime of the MM computed for $P = 150$. In agreement with the asymptotic analysis, we observe that both the MM and UML show a roughly linear trend over P, although with different slopes. On the other hand, the ML 2D exhibits a superlinear trend, with considerably longer runtimes compared with those of the MM and UML, and a complexity which becomes prohibitive as P increases.

IV. Multiple-Input Single-Output (MISO): Fundamental Bounds

In this section, we derive the Fisher Information Matrix (FIM) and the CRLB for the problem of MS position estimation. We start by deriving the bounds on the channel parameters, namely, TOF τ, AOD θ, and path gain α. Then, we transform these bounds into the position domain.

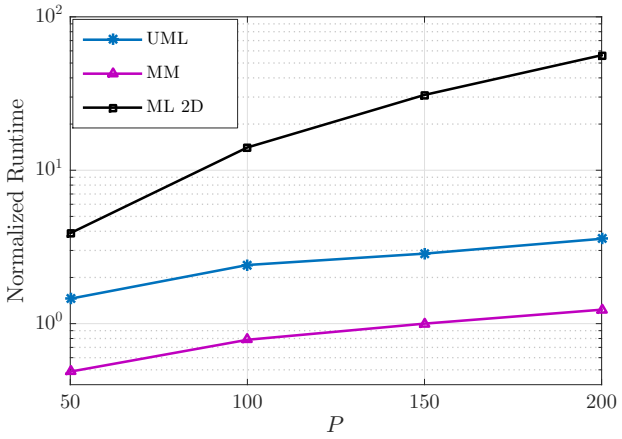

Fig. 3: Runtimes as function of the number of grid points.

A. FIM Derivation for Channel Parameters

Let the noise-free observation at subcarrier n, transmission g be

$$m^g[n] = \sqrt{N_{\text{BS}}}\alpha \exp\left(\frac{-j2\pi n\tau}{NT_s}\right)\boldsymbol{a}^H(\theta)\boldsymbol{s}^g[n]$$

where $\boldsymbol{s}^g[n] = \boldsymbol{F}^g[n]\boldsymbol{x}^g[n]$, $\alpha = h/\sqrt{\rho} \overset{\text{def}}{=} r\exp(j\phi)$ with r and ϕ modulus and phase of the complex amplitude α, respectively. Let $\boldsymbol{\gamma} \in \mathbb{R}^{4\times 1}$ denotes the vector of the unknown channel parameters

$$\boldsymbol{\gamma} = [r \ \phi \ \tau \ \theta]^{\text{T}} \tag{40}$$

where we assume without loss of generality that the noise variance σ^2 is known[5]. Defining $\hat{\boldsymbol{\gamma}}$ as an unbiased estimator of $\boldsymbol{\gamma}$, it is well-known that the mean squared error (MSE) is lower bounded as [43]

$$\mathbb{E}_{\boldsymbol{Y}|\boldsymbol{\gamma}}\left[(\hat{\boldsymbol{\gamma}}-\boldsymbol{\gamma})(\hat{\boldsymbol{\gamma}}-\boldsymbol{\gamma})^{\text{T}}\right] \succeq \boldsymbol{J}_{\boldsymbol{\gamma}}^{-1} \tag{41}$$

where $\mathbb{E}_{\boldsymbol{Y}|\boldsymbol{\gamma}}[\cdot]$ denotes the expectation parameterized as function of the unknown vector $\boldsymbol{\gamma}$ and $\boldsymbol{J}_{\boldsymbol{\gamma}}$ is the 4×4 FIM defined as [44]

$$\begin{aligned}\boldsymbol{J}_{\boldsymbol{\gamma}} &= \mathbb{E}_{\boldsymbol{Y}|\boldsymbol{\gamma}}\left[-\frac{\partial^2 \log f(\boldsymbol{Y}|\boldsymbol{\gamma})}{\partial\boldsymbol{\gamma}\partial\boldsymbol{\gamma}^{\text{T}}}\right] \\ &= \frac{2}{\sigma^2}\sum_{g=1}^{G}\sum_{n=0}^{N-1}\Re\left\{\nabla m^g[n]\nabla^{\text{H}} m^g[n]\right\}\end{aligned} \tag{42}$$

where $f(\boldsymbol{Y}|\boldsymbol{\gamma})$ is the conditional likelihood function of $\boldsymbol{Y}$ given $\boldsymbol{\gamma}$, while $\nabla m^g[n]$ is the gradient of m with respect to $\boldsymbol{\gamma}$ given by

$$\nabla m^g[n] = \begin{bmatrix} \sqrt{N_{\text{BS}}}\exp(j\phi)\exp\left(\frac{-j2\pi n\tau}{NT_s}\right)\boldsymbol{a}^{\text{H}}(\theta)\boldsymbol{s}^g[n] \\ j\sqrt{N_{\text{BS}}}\alpha\exp\left(\frac{-j2\pi n\tau}{NT_s}\right)\boldsymbol{a}^{\text{H}}(\theta)\boldsymbol{s}^g[n] \\ \frac{-j2\pi n}{NT_s}\sqrt{N_{\text{BS}}}\alpha\exp\left(\frac{-j2\pi n\tau}{NT_s}\right)\boldsymbol{a}^{\text{H}}(\theta)\boldsymbol{s}^g[n] \\ \frac{-j2\pi}{\lambda_c}d\cos\theta\sqrt{N_{\text{BS}}}\alpha\exp\left(\frac{-j2\pi n\tau}{NT_s}\right)\boldsymbol{a}^{\text{H}}(\theta)\boldsymbol{B}\boldsymbol{s}^g[n]\end{bmatrix}$$

with $\Re\{\cdot\}$ denoting the real-part operator and $\boldsymbol{B} = \text{diag}[0\ 1\ \cdots\ (N_{\text{BS}}-1)]$, where $\text{diag}(\cdot)$ construct a diagonal matrix with its entries. We can show that for the matrix $\boldsymbol{J}_{\boldsymbol{\gamma}}$ to be non-singular when $G = 1$, we need at least two subcarriers and send different pilot sequences on each subcarrier. Similarly, when $N = 1$, we need at least two transmissions with different pilot sequences. Further details are found in the Appendix.

[5]We recall that if σ^2 were unknown, it could be estimated using the equation provided above (19).

B. FIM Derivation for Position

In this section, we derive the FIM in the position domain by applying a transformation of variables from the vector of channel parameters $\boldsymbol{\gamma}$ to the vector of location parameters

$$\boldsymbol{\eta} = [r \ \phi \ p_x \ p_y]^{\text{T}}. \tag{43}$$

The FIM of $\boldsymbol{\eta}$ is obtained by means of the 4×4 transformation matrix $\boldsymbol{T}$ as

$$\boldsymbol{J}_{\boldsymbol{\eta}} = \boldsymbol{T}\boldsymbol{J}_{\boldsymbol{\gamma}}\boldsymbol{T}^{\text{T}} \tag{44}$$

where

$$\boldsymbol{T} \overset{\text{def}}{=} \frac{\partial\boldsymbol{\gamma}^{\text{T}}}{\partial\boldsymbol{\eta}} = \begin{bmatrix} \partial r/\partial r & \partial\phi/\partial r & \partial\tau/\partial r & \partial\theta/\partial r \\ \partial r/\partial\phi & \partial\phi/\partial\phi & \partial\tau/\partial\phi & \partial\theta/\partial\phi \\ \partial r/\partial p_x & \partial\phi/\partial p_x & \partial\tau/\partial p_x & \partial\theta/\partial p_x \\ \partial r/\partial p_y & \partial\phi/\partial p_y & \partial\tau/\partial p_y & \partial\theta/\partial p_y \end{bmatrix}. \tag{45}$$

The entries of the matrix $\boldsymbol{T}$ can be obtained from the relations between the parameters in $\boldsymbol{\gamma}$ and $\boldsymbol{\eta}$, as expressed in (9)–(10). More precisely, we have

$$\partial r/\partial r = \partial\phi/\partial\phi = 1,$$

$$\partial\tau/\partial p_x = \frac{p_x}{c(p_x^2+p_y^2)^{-\frac{1}{2}}}, \qquad \partial\tau/\partial p_y = \frac{p_y}{c(p_x^2+p_y^2)^{-\frac{1}{2}}},$$

$$\partial\theta/\partial p_x = \frac{-p_y/p_x^2}{1+(p_y/p_x)^2}, \qquad \partial\theta/\partial p_y = \frac{1/p_x}{1+(p_y/p_x)^2},$$

and the rest of the entries in $\boldsymbol{T}$ are zero.

C. Bounds on Position Estimation Error

The position error bound (PEB) can be readily derived by inverting the FIM $\boldsymbol{J}_{\boldsymbol{\eta}}$ given in (44), then adding the diagonal entries of the lower right 2×2 sub-matrix, and taking the square root as

$$\text{PEB} = \sqrt{[(\boldsymbol{J}_{\boldsymbol{\eta}})^{-1}]_{3,3} + [(\boldsymbol{J}_{\boldsymbol{\eta}})^{-1}]_{4,4}} \tag{46}$$

where the operator $[\cdot]_{j,j}$ denotes the selection of the j-th diagonal entry of $\boldsymbol{J}_{\boldsymbol{\eta}}^{-1}$.

V. Simulation Model and Results

In this section, we present simulation results to evaluate the performance of the proposed estimators in comparison with the two-dimensional ML, as well as the theoretical bounds derived based on the FIM analysis conducted in Sec. IV.

A. Reference scenario

We consider a scenario representative of outdoor localization in a small open area with maximum distance between BS and MS of 20 meters. The BS is located at known position $[3\ 0]^{\mathrm{T}}$ [m] of the considered Cartesian reference system and is equipped with $N_{\mathrm{BS}} = 10$ antennas, while the MS is initially placed at $\boldsymbol{p} = [5\ 15]^{\mathrm{T}}$ [m]. As concerns the transmitted signal, we assume a carrier frequency $f_c = 60$ GHz, a bandwidth $B = 40$ MHz, a transmitted power $P_t = 1$ W (30 dBm, a typical value for local area BS [45]), and a number of subcarriers $N = 20$ [46]. The number of simultaneously transmitted beams is $M = 1$ and we vary the number of sequentially transmitted signals G between 1 and 20.

The channel path loss ρ is computed according to [47], [48]. For the specific case of the LOS link, we obtain

$$1/\rho = \mu^2(d_0)\left(\frac{\lambda_c}{4\pi d_0}\right)^2 \tag{47}$$

where $\mu^2(d_0)$ denotes the atmospheric attenuation at a distance d_0 and the last term is the free space path loss at a distance d_0. Following [1], the atmospheric attenuation $\mu^2(d_0)$ is set to 16 dB/Km. As to the complex channel gain, it can be expressed in terms of $h = a\mathrm{e}^{j\varphi}$ with $a = \sqrt{P_t}$ the amplitude and φ the related phase, respectively.

To complete the analysis, we show the performance achievable in the uplink channel and compare them with the ones obtained in the downlink. Notice that, in the uplink case, the model of the received signal is different from the one provided in (7) since an antenna array should be considered at the receiver side. As a result, the localization will be based on the estimation of the AOA, as typical in many existing approaches, while we recall that the present contribution focuses on leveraging AOD information. Therefore, in the following we will consider the proper modified expressions for the theoretical bounds, as derived in the literature [11].

As anticipated in Sec. III-A, we also investigate the performance of the proposed estimators in presence of multipath propagation. Notice that, in this case, the estimation performance is evaluated in a simulation environment that is not matched to the design assumption of the proposed algorithms. More precisely, it is assumed that, in addition to the direct LOS link, two different NLOS paths are present at the receiver side. Assuming that only one dominant reflector is present in each NLOS path [48], we can compute the path loss ρ_k for the k-th NLOS link with path length d_k according to

$$1/\rho_k = \sigma_0^2 \mathbb{P}_0(d_k)\left(\frac{\lambda_c}{4\pi d_k}\right)^2 \tag{48}$$

where $\mathbb{P}_0(d_k) = (\gamma_r d_k)^2 \mathrm{e}^{-\gamma_r d_k}$ denotes the Poisson distribution of the environment geometry with density γ_r, and $k = 1, 2$. According to [48], we consider a density $\gamma_r = 1/7$ and set the average reflection loss for the first-order reflection σ_0^2 to 10 dB with the root-mean-square (RMS) deviation equal to 4 dB. To analyze the sensitivity of the proposed estimators to multipath effects, we consider the following definition of LMR:

$$\mathrm{LMR} = \frac{P_{\mathrm{LOS}}}{\sum_{k=1}^{2} P_{\mathrm{NLOS}}^k} = \frac{1/\rho}{1/\rho_1 + 1/\rho_2} \tag{49}$$

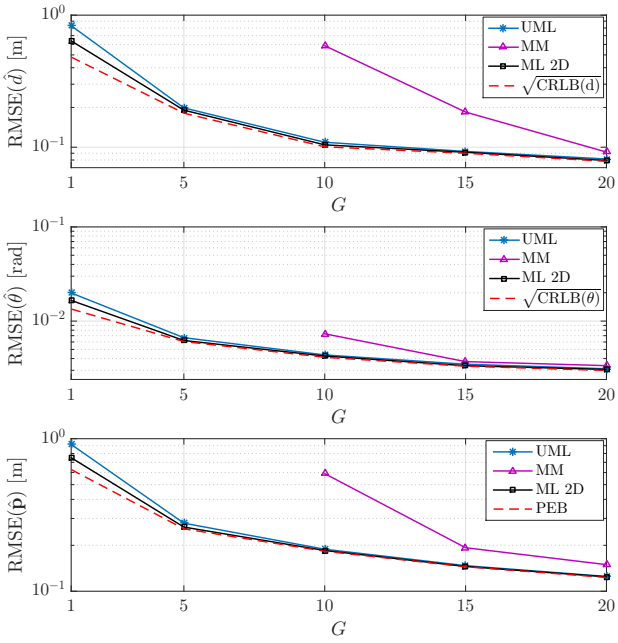

Fig. 4: RMSEs of the estimated d, θ, and $\boldsymbol{p}$ versus CRLBs as function of the transmissions G for SNR = 5 dB in LOS condition.

where P_{LOS} is the power associated to the LOS path, while P_{NLOS}^k is the power of the k-th multipath component.

The elements of the analog beamformers $\boldsymbol{F}_{\mathrm{RF}}$ are generated as uniform random values on the unit circle. Since we are not dealing with the design of beamformers, in the analysis we assume a number of RF chains equal to 10, but the proposed techniques are general and can be particularized to any specific design of beamformers. As concerns the sequences $\bar{\mathbf{x}}^g[n] = \mathbf{F}_{\mathrm{BB}}^g[n]\mathbf{x}^g[n]$, they are computed as complex exponential terms $\mathrm{e}^{j\phi_{n,g}}$ having random phases uniformly distributed in $[0, 2\pi)$ along different subcarriers n and different transmissions g, respectively. Finally, we define the SNR in dB as

$$\mathrm{SNR} \overset{\mathrm{def}}{=} 10\log_{10}\left(\frac{P_t}{\rho N_0 B}\right) \tag{50}$$

where $\log_{10}(\cdot)$ denotes the base-10 logarithm and $N_0 B$ is the receiver noise figure, i.e., $N_0 B = k_B T_0 B$, k_B being the Boltzmann constant and T_0 the standard thermal noise temperature.

We consider the Root Mean Squared Error (RMSE) as metric to assess the algorithms performance, estimated based on 1000 Monte Carlo trials.

B. AOD, TOF and Position Estimation in LOS

In this section, we assess the performance of the proposed algorithms assuming only the LOS component is present.

In Fig. 4 we depict the RMSE of the estimated values of $d = c\tau$, θ and $\boldsymbol{p}$ as function of the number of transmissions G for SNR = 5 dB, compared against the theoretical bounds derived based on the FIM analysis in Sec. IV. More precisely, the values of $\sqrt{\mathrm{CRLB}(\cdot)}$ are obtained similarly to the PEB defined in (46), i.e., by inverting the FIM $\boldsymbol{J}_{\boldsymbol{\gamma}}$ from (42), choosing the corresponding diagonal entries and taking the

square root. For comparison, we have also added the performance of the two-dimensional ML estimator in (22). For the implementation of the MM algorithm, we compared the one-lag based estimator in (38) with the multi-lag extension in (39), assuming a number of lags $L = 2$. We observed that both estimators exhibit almost the same performance in the considered scenario.

As it can be seen from Fig. 4, the UML algorithm converges to the corresponding bounds for almost all the considered values of transmissions G. Remarkably, it exhibits very good estimation performance even in case of $G = 1$, achieving the same accuracy as the two-dimensional ML estimator, but at a significantly reduced computational cost.

Starting from a sufficient number of transmissions $G = 10$ — which we recall is the limit condition for defining the right pseudoinverse $\boldsymbol{X}_i^+$ required in (34) — we can observe that the performance of the MM estimator is worse than that of the UML, but still acceptable in terms of achieved accuracy. As the solid (magenta) curves show, the RMSE of $\hat{d}$ exhibits a small gap with respect to the theoretical lower bound, which however starts to decrease as more transmissions G are available, thanks to an increasingly accurate estimation of the first-order moment in (37). On the other hand, the RMSE of $\hat{\theta}$ approaches the theoretical bounds for $G \geq 15$. As the bottom plot in Fig. 4 shows, this results in an overall position error which is always below 60 cm and tends to decrease as G increases, achieving performance very close to the one provided by the UML, but at the lower cost of a single one-dimensional search.

It is worth noticing that the total transmitted energy is not fixed and independent of the number of transmissions G, but increases with G. Thus, the RMSE decreases with $1/\sqrt{G}$ due to the availability of more data in the estimation process. Just to give a concrete example, in the interval $G \in [10, 20]$ the RMSE drops by a factor of $1/\sqrt{2}$, that is, it decreases since the transmitted energy grows with G (in the specific case, it doubles).

Fig. 5 shows the evolution of the RMSEs of d, θ and $\boldsymbol{p}$ with respect to different values of the received SNR for the challenging case of $G = 1$ in both uplink and downlink channels. It is worth noting that, in this case, the pseudoinverse matrix $\boldsymbol{X}_i^+$ in (34) is not defined and hence the MM estimator cannot be implemented. By comparing the obtained results, it can be seen that a higher estimation accuracy is achieved in the uplink channel. This behavior can be linked to the fact that, in the uplink channel, a N_{BS}-dimensional vector of samples is available for each subcarrier, thus resulting in better estimation conditions with respect to the downlink channel, as confirmed by the smaller values of the bounds (dashed-dot red curves).

Interestingly, the proposed UML estimator performs well even for very low values of the received SNR, which is a typical operating condition in mmWave systems before beamforming stage. On the other hand, it should be noticed that the UML attains the theoretical bounds also in the downlink channel, starting from values of SNR of about 10 dB.

In addition to a direct comparison on the achievable performance, there are several aspects that should be jointly considered when comparing uplink and downlink localization

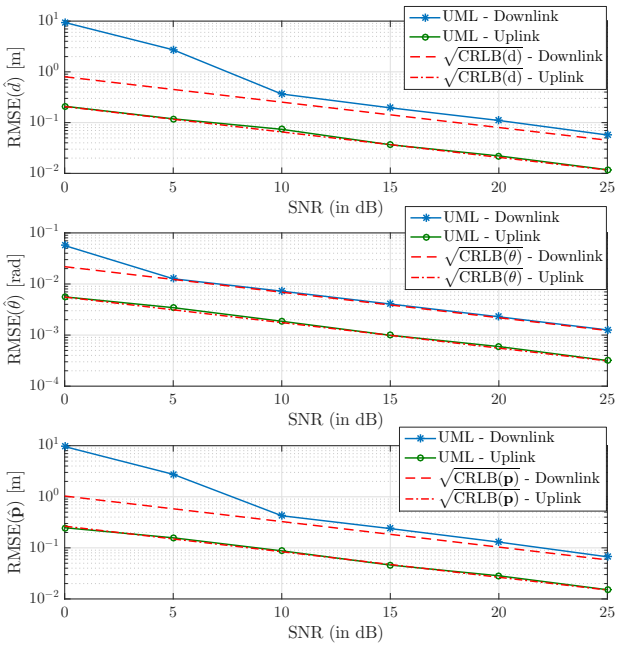

Fig. 5: RMSEs of the estimated d, θ, and $\boldsymbol{p}$ versus CRLBs as function of the SNR for $G = 1$ in LOS condition for both uplink and downlink channels.

from a system perspective. More precisely, it should be observed that, in general, the power budget in the uplink is lower than that experienced in the downlink, which in turn results in much lower values of the SNR. Furthermore, localization exploiting the uplink channel would require that proper resource allocation techniques are implemented at the BSs. The main drawback of such techniques consists in the fact that the maximum number of served users is usually fixed during the deployment phase and cannot be easily updated over time. Moreover, the storage of sensitive data (positions of users) raises a number of additional issues concerning legal aspects related to both privacy and data protection. Conversely, the downlink channel is characterized by better SNR conditions and allows multiple (potentially unlimited) users to be localized by exploiting broadcast signals. In doing so, the additional issues related to both resource allocation and data protection are completely avoided. We however remark that an exhaustive comparison between downlink and uplink localization should include other aspects that are beyond the scope of the present contribution.

C. AOD, TOF and Position Estimation in LOS + NLOS

In this section, we evaluate the algorithms performance assuming that, in addition to the direct LOS path, two NLOS paths due to multipath propagation are also present. To analyze how the positions of the reflectors impact the ultimate performance of the proposed algorithms, we investigate the following two different scenarios:

- In a first setup, we keep fixed the positions of BS and MS and assume the two reflectors are placed at $[0\ 7]^{\text{T}}$ [m] and $[10\ 6]^{\text{T}}$ [m], respectively. Under this scenario, the AOD related to the LOS path is equal to $\theta_0 = 77°$ and the

TOF τ_0 is such that the distance between the BS and MS $d_0 = c\tau_0 = 15.1$ meters. As concerns the NLOS channel parameters, the two AODs are $\theta_1 = 41^\circ$ and $\theta_2 = 113^\circ$, while the related delays are such that $d_1 = d_{1,1} + d_{1,2} = c\tau_1 = 19.5$ meters and $d_2 = d_{2,1} + d_{2,2} = c\tau_2 = 17$ meters, respectively;

- In a second setup, we move the MS closer to the second reflector, that is, we set $\boldsymbol{p} = [10\ 8]^{\mathrm{T}}$ [m]. In this case, $\theta_0 = 48^\circ$ while the TOF τ_0 is such that $d_0 = 10.6$ meters. Clearly, the AODs of the two NLOS paths remain the same while the related delays change according to the variation in the MS position, that is, they are such that $d_1 = 11.2$ meters and $d_2 = 17.7$ meters, respectively.

As it can be noticed, the first scenario corresponds to a more favorable case where LOS and NLOS paths are well-separated in both time and space domains. Conversely, the second setup is more challenging since both θ_0 and τ_0 are very close to θ_2 and τ_2, hence the LOS link cannot be easily distinguished from the NLOS path generated by the second reflector.

1) Well-separated paths: In Fig. 6a we report the RMSEs of d, θ and $\boldsymbol{p}$ as function of different levels of LMR for $G = 10$ and SNR = 15 dB assuming the LOS and NLOS paths are well-separated. As it could be expected, the obtained performance is worse than that in LOS-only (depicted as dashed curves for reference), especially for non-negligible levels of multipath power. Nevertheless, a high level of position accuracy can still be achieved for mid to high values of LMR, with the UML algorithm exhibiting the same estimation performance of the more computationally demanding ML 2D. The localization capability of the MM algorithm is also interesting, at least for non-severe multipath, as confirmed by the solid (magenta) curves.

2) Closely-spaced paths: In Fig. 6b we report the RMSEs of d, θ and $\boldsymbol{p}$ for the same values of the parameters assumed in the previous case, but in the more challenging scenario where the LOS link cannot be easily distinguished from the NLOS path generated by the second reflector. Interestingly, the obtained results reveals that the proposed approaches can correctly cope also with the presence of NLOS paths that are very close (in both time and space) to the LOS link, with a slight degradation of the achieved performance only for small values of the LMR. These results show that the proposed algorithms are effective also in presence of multipath propagation.

VI. Conclusion

We have addressed the problem of determining the unknown MS position in a mmWave MISO system based on the AOD of received downlink signals. Such a setup has several attractive properties compared to the more conventional uplink case; in particular, AOD can be conveniently estimated using a single receive antenna, thus providing an efficient way for locating a receiver while avoiding the complexity of large arrays. We have performed a thorough theoretical analysis, providing the exact solution to the ML estimation problem and deriving the fundamental lower bounds on the estimation uncertainty for both channel and position parameters. To circumvent the need for multidimensional optimization of the joint ML estimator, we proposed two novel estimators more amenable to practical implementation. The performance assessment demonstrated that different accuracy/complexity trade-offs exist; however, remarkably, it is possible to achieve almost the same performance of the exact ML estimator, at a fraction of its computational burden, even in presence of few transmissions, low SNRs, and multipath propagation effects. Our work shows that low-complexity estimation of delay and AOD is indeed possible with a single receive antenna, provided at least two distinct (either in time or frequency) signals are sent by a multi-antenna transmitter.

Appendix

Necessary conditions for non-singular FIM

For clarity, we drop τ from the unknowns and consider the case $G = 1$ (allowing us to drop the index g), and introduce

$$\zeta[n] = \boldsymbol{a}^{\mathrm{H}}(\theta)\boldsymbol{s}[n]$$
$$\xi[n] = \boldsymbol{a}^{\mathrm{H}}(\theta)\boldsymbol{B}\boldsymbol{s}[n],$$

from which we create length N vectors

$$\boldsymbol{\zeta} = \boldsymbol{S}^{\mathrm{T}}\boldsymbol{a}^*(\theta) \tag{51}$$
$$\boldsymbol{\xi} = \boldsymbol{S}^{\mathrm{T}}\boldsymbol{B}\boldsymbol{a}^*(\theta), \tag{52}$$

where $\boldsymbol{S}$ has as columns the N pilots $\boldsymbol{s}[n]$. The FIM is then given by (up to irrelevant constants)

$$\boldsymbol{J}_{\boldsymbol{\gamma}} \propto \sum_{n=0}^{N-1} \Re\{\nabla m[n] \nabla^{\mathrm{H}} m[n]\} \tag{53}$$

$$\nabla m[n] \propto [\zeta[n],\ jr\zeta[n],\ -j\kappa\pi\cos\theta r\xi[n]]^{\mathrm{T}} \tag{54}$$

where $\kappa = 2d\cos\theta/\lambda_c$. Substitution of (54) into (53) yields

$$\boldsymbol{J}_{\boldsymbol{\gamma}} \propto \begin{bmatrix} \boldsymbol{\zeta}^{\mathrm{H}}\boldsymbol{\zeta} & 0 & r\kappa\Im(\boldsymbol{\xi}^{\mathrm{H}}\boldsymbol{\zeta}) \\ 0 & r^2\boldsymbol{\zeta}^{\mathrm{H}}\boldsymbol{\zeta} & r^2\kappa\Re(\boldsymbol{\xi}^{\mathrm{H}}\boldsymbol{\zeta}) \\ r\kappa\Im(\boldsymbol{\xi}^{\mathrm{H}}\boldsymbol{\zeta}) & r^2\kappa\Re(\boldsymbol{\xi}^{\mathrm{H}}\boldsymbol{\zeta}) & r^2\kappa^2\boldsymbol{\xi}^{\mathrm{H}}\boldsymbol{\xi} \end{bmatrix}$$

where $\Im\{\cdot\}$ denotes the imaginary-part operator. This matrix is full-rank if and only if its determinant is non-zero. Computing the determinant, we find that all terms are proportional to $\boldsymbol{\zeta}^{\mathrm{H}}\boldsymbol{\zeta} r^4\kappa^2$, so that

$$\begin{aligned} \det \boldsymbol{J}_{\boldsymbol{\gamma}} = 0 &\iff \boldsymbol{\zeta}^{\mathrm{H}}\boldsymbol{\zeta}\boldsymbol{\xi}^{\mathrm{H}}\boldsymbol{\xi} - (\Re(\boldsymbol{\xi}^{\mathrm{H}}\boldsymbol{\zeta}))^2 - (\Im(\boldsymbol{\xi}^{\mathrm{H}}\boldsymbol{\zeta}))^2 = 0 \\ &\iff \|\boldsymbol{\zeta}\|^2\|\boldsymbol{\xi}\|^2 = |\boldsymbol{\xi}^{\mathrm{H}}\boldsymbol{\zeta}|^2. \end{aligned}$$

From the Cauchy-Schwarz inequality for complex numbers, it then follows that the FIM is singular if and only if $\boldsymbol{\zeta}$ and $\boldsymbol{\xi}$ are parallel, i.e., there exists a $u \in \mathbb{C}$ so that $\boldsymbol{\xi} = u\boldsymbol{\zeta}$. It then follows immediately that:

- when $N = 1$, $\boldsymbol{\zeta}$ and $\boldsymbol{\xi}$ become scalars, which are necessarily parallel and thus $\boldsymbol{J}_{\boldsymbol{\gamma}}$ is singular;
- when $N > 1$, a necessary and sufficient condition for a non-singular $\boldsymbol{J}_{\boldsymbol{\gamma}}$ is that the columns of $\boldsymbol{S}$ are not parallel.

Thus, a necessary and sufficient condition for a non-singular FIM with a single transmission ($G = 1$) is that we use at least $N = 2$ subcarriers and that the pilots across those subcarriers are different (non parallel). It can similarly be shown that when $N = 1$, we must use at least two transmissions with different pilots.

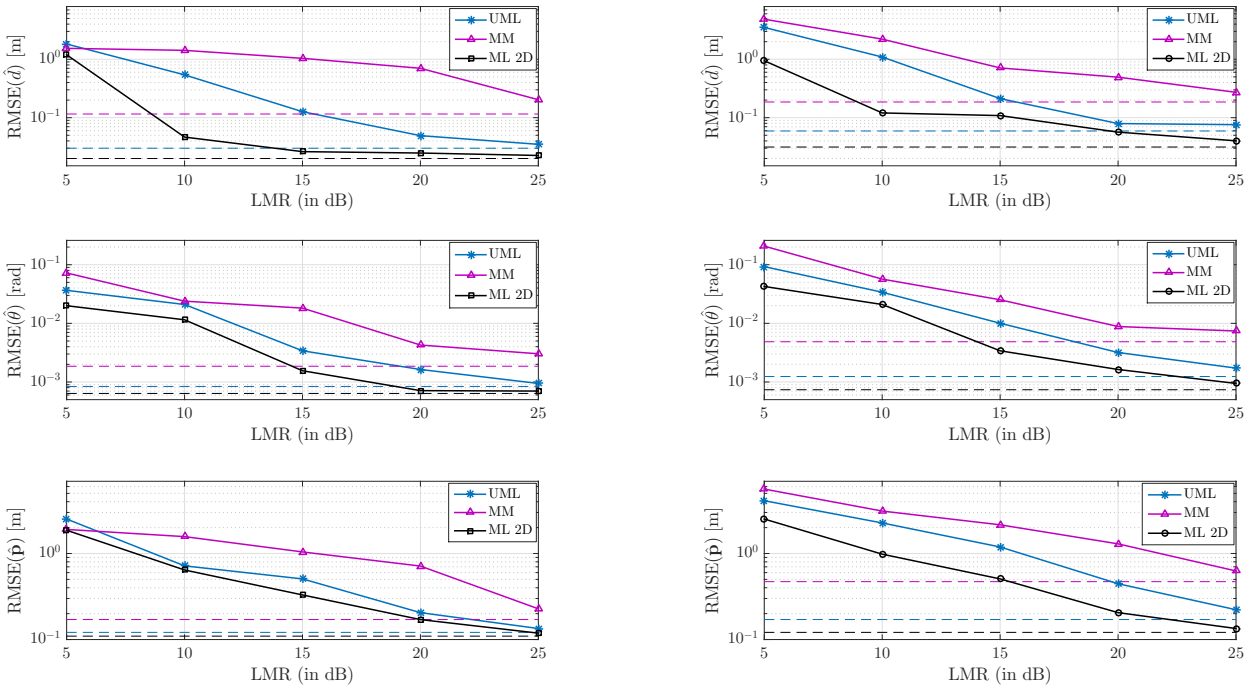

(a) Well-separated paths.

(b) Closely-spaced paths.

Fig. 6: RMSEs of the estimated d, θ, and $\boldsymbol{p}$ as function of the LMR for $G = 10$ and SNR = 15 dB for (a) well-separated and (b) closely-spaced paths. The dashed-curves represent LOS performance for reference.

REFERENCES

[1] T. Rappaport, S. Sun, R. Mayzus, H. Zhao, Y.Azar, K.Wang, G.Wong, J. Schulz, M. Samimi, and F. Gutierrez, "Millimeter wave mobile communications for 5G cellular: It will work!", *IEEE Access*, Vol. 1, pp. 335–349, May 2013.

[2] L. Lu, G. Y. Li, A. L. Swindlehurst, A. Ashikhmin, and R. Zhang, "An overview of massive MIMO: Benefits and challenges", *IEEE J. Sel. Topics Signal Processing*, Vol. 8, No. 5, pp. 742–758, May 2014.

[3] E. G. Larsson, O. Edfors, F. Tufvesson, and T. L. Marzetta, "Massive MIMO for next generation wireless systems," *IEEE Communications Magazine*, Vol. 52, No. 2, pp. 186–195, February 2014.

[4] T. Bai and R. Heath, "Coverage and rate analysis for millimeter-wave cellular networks," *IEEE Trans. Wireless Commun.*, Vol. 14, No. 2, pp. 1100–1114, Feb. 2015.

[5] M. Akdeniz et al., "Millimeter wave channel modeling and cellular capacity evaluation," *IEEE J. Sel. Areas Commun.*, Vol. 32, No. 6, pp. 1164–1179, Jun. 2014.

[6] R. D. Taranto, S. Muppirisetty, R. Raulefs, D. Slock, T. Svensson, and H. Wymeersch, "Location-aware communications for 5G networks: How location information can improve scalability, latency, and robustness of 5G", *IEEE Signal Process. Mag*, Vol. 31, No. 6, pp. 102–112, Nov. 2014.

[7] N. Garcia, H. Wymeersch, E. G. Ström, and D. Slock, "Location-aided mm-wave channel estimation for vehicular communication", *IEEE 17th Int. Workshop on Signal Process. Advances in Wireless Commun.*, Edinburgh, pp. 1–5, July 2016.

[8] K. Witrisal, P. Meissner, E. Leitinger, Y. Shen, C. Gustafson, F. Tufvesson, K. Haneda, D. Dardari, A. F. Molisch, A. Conti, and M. Z. Win, "High-accuracy localization for assisted living: 5G systems will turn multipath channels from foe to friend", *IEEE Signal Process. Mag*, Vol. 33, No. 2, pp. 59–70, March 2016.

[9] G. Destino, H. Wymeersch, "On the trade-off between positioning and data rate for mm-wave communication", *IEEE Int. Conf. Commun. Workshops (ICCW)*, pp. 797–802, May 2017.

[10] A. Guerra, F. Guidi and D. Dardari, "Single-Anchor Localization and Orientation Performance Limits Using Massive Arrays: MIMO vs Beamforming," *IEEE Trans. Wireless Commun.*, Vol. 17, No. 8, pp. 5241–5255, Aug. 2018.

[11] Z. Abu-Shaban, X. Zhou, T. Abhayapala, G. Seco-Granados, and H. Wymeersch, "Error Bounds for Uplink and Downlink 3D Localization in 5G Millimeter Wave Systems," *IEEE Trans. Wireless Commun.*, Vol. 17, No. 8, pp. 4939–4954, Aug. 2018.

[12] R. Mendrzik, H. Wymeersch, G. Bauch, and Z. Abu-Shaban, "Harnessing NLOS Components for Position and Orientation Estimation in 5G mmWave MIMO", *IEEE Trans. on Wireless Commun.*, Vol. 18, No. 1, pp. 93–107, Jan. 2019.

[13] A. Shahmansoori, G. E. Garcia, G. Destino, G. Seco-Granados and H. Wymeersch, "Position and Orientation Estimation Through Millimeter-Wave MIMO in 5G Systems", *IEEE Trans. Wireless Commun.*, Vol. 17, No. 3, pp. 1822–1835, March 2018.

[14] Z. Lin, T. Lv and P. T. Mathiopoulos, "3-D Indoor Positioning for Millimeter-Wave Massive MIMO Systems", *IEEE Transactions on Communications*, Early Access, Jan. 2018.

[15] H. Deng and A. Sayeed, "Mm-wave MIMO channel modeling and user localization using sparse beamspace signatures," *IEEE 15th International Workshop on Signal Processing Advances in Wireless Communications (SPAWC)*, Toronto, ON, pp. 130–134, June 2014.

[16] A. Hu, T. Lv, H. Gao, Z. Zhang and S. Yang, "An ESPRIT-Based Approach for 2-D Localization of Incoherently Distributed Sources in Massive MIMO Systems," *IEEE J. Sel. Topics Signal Processing*, Vol. 8, No. 5, pp. 996–1011, Oct. 2014.

[17] M. Koivisto et al., "Joint device positioning and clock synchronization in 5G ultra-dense networks," *IEEE Trans. Wireless Commun.*, Vol. 16, No. 5, pp. 2866–2881, May 2017.

[18] N. Garcia, H. Wymeersch, E. G. Larsson, A. M. Haimovich, and M. Coulon, "Direct localization for massive MIMO," *IEEE Trans. Signal Process.*, Vol. 65, No. 10, pp. 2475–2487, May 2017.

[19] A. Guerra, F. Guidi, and D. Dardari, "Position and orientation error bound for wideband massive antenna arrays," *Proc. Int. Conf. Commun. Workshop (ICC)*, London, U.K., pp. 853–858, Jun. 2015.

[20] J. Li, J. Conan, and S. Pierre, "Position location of mobile terminal in wireless MIMO communication systems," *Journ. Commun. Netw.*, Vol. 9, No. 3, pp. 254–264, Sep. 2007.

[21] V. Savic and E. G. Larsson, "Fingerprinting-based positioning in distributed massive MIMO systems," *IEEE Veh. Technol. Conf. (VTC)*, Boston, USA, pp. 1–5, Sep. 2015.

[22] A. M. Sayeed, "Deconstructing multiantenna fading channels," *IEEE Trans. Signal Process.*, Vol. 50, No. 10, pp. 2563–2579, Oct. 2002.

[23] K. Cengiz and M. Aydemir, "Next-Generation Infrastructure and Technology Issues in 5G Systems," *Journal of Commun. Soft. and Sys.*, Vol. 4, No. 1, pp. 33–39, March. 2018.

[24] D. Gesbert, M. Kountouris, R. W. Heath, C. Chae, and T. Salzer, "Shifting the MIMO Paradigm," *IEEE Signal Process. Mag.*, Vol. 24, No. 5, pp. 36–46, Sept. 2007.

[25] T. L. Marzetta, "Noncooperative Cellular Wireless with Unlimited Numbers of Base Station Antennas," *IEEE Trans. Wireless Commun.*, Vol. 9, No. 11, pp. 3590–3600, Novemb. 2010.

[26] M. Wax and A. Leshem, "Joint estimation of time delays and directions of arrival of multiple reflections of a known signal," *IEEE International Conference on Acoustics, Speech, and Signal Processing (ICASSP)*, Atlanta, GA, USA, Vol. 5, pp. 2622–2625, 1996.

[27] A. L. Swindlehurst, "Time Delay and Spatial Signature Estimation Using Known Asynchronous Signals", *IEEE Transactions on Signal Processing*, Vol. 46, No. 2, pp. 449–462, Feb. 1998.

[28] A. L. Swindlehurst, P. Stoica, "Maximum Likelihood Methods in Radar Array Signal Processing", *Proc. of the IEEE*, Vol. 86, no 2, pp. 421–441, Feb. 1998.

[29] T. Bai and R. W. Heath, "Analysis of self-body blocking effects in millimeter wave cellular networks," *48th Asilomar Conference on Signals, Systems and Computers*, Pacific Grove, CA, pp. 1921–1925, Nov. 2014.

[30] A. Ravanshid et al., "Multi-connectivity functional architectures in 5G," *IEEE International Conference on Communications Workshops (ICC)*, Kuala Lumpur, pp. 187–192, May 2016.

[31] M. Giordani, M. Mezzavilla, S. Rangan and M. Zorzi, "Multi-connectivity in 5G mmWave cellular networks," *Medit. Ad Hoc Network. Workshop (Med-Hoc-Net)*, Vilanova i la Geltru, pp. 1–7, June 2016.

[32] V. Petrov et al., "Dynamic Multi-Connectivity Performance in Ultra-Dense Urban mmWave Deployments," *IEEE Journal on Selected Areas in Communications*, Vol. 35, No. 9, pp. 2038–2055, Sept. 2017.

[33] A. Alkhateeb and R. W. Heath, "Frequency Selective Hybrid Precoding for Limited Feedback Millimeter Wave Systems", *IEEE Transactions on Communications*, Vol. 64, No. 5, pp. 1801–1818, May 2016.

[34] J. Brady, N. Behdad, and A. M. Sayeed, "Beamspace MIMO for Millimeter-Wave Communications: System Architecture, Modeling, Analysis, and Measurements", *IEEE Transactions on Antennas and Propagation*, Vol. 61, No. 7, pp. 3814–3827, July 2013.

[35] J. H. Brady and A. M. Sayeed, "Wideband communication with high-dimensional arrays: New results and transceiver architectures", *IEEE International Conference on Communication Workshop (ICCW)*, London, pp. 1042–1047, June 2015.

[36] Y. Shen and M. Z. Win, "Fundamental Limits of Wideband Localization — Part I: A General Framework," *IEEE Transactions on Information Theory*, Vol. 56, No. 10, pp. 4956–4980, Oct. 2010.

[37] Y. Shen, H. Wymeersch, and M. Z. Win, "Fundamental limits of wideband localization — Part II: Cooperative networks," *IEEE Transactions on Information Theory*, Vol. 56, No. 10, pp. 4981–5000, Oct 2010.

[38] Y. Han, Y. Shen, X. Zhang, M. Z. Win and H. Meng, "Performance Limits and Geometric Properties of Array Localization," *IEEE Transactions on Information Theory*, Vol. 62, No. 2, pp. 1054–1075, Feb. 2016.

[39] Z. Abu-Shaban, H. Wymeersch, T. Abhayapala, and G. Seco-Granados, "Single-Anchor Two-Way Localization Bounds for 5G mmWave Systems: Two Protocols", [online] Available: https://arxiv.org/abs/1805.02319.

[40] V. Sark, E. Grass and J. Gutierrez, "Multi-Way ranging with clock offset compensation," *Advances in Wireless and Optical Communications (RTUWO)*, Riga, pp. 68–71, Nov. 2015.

[41] S. Kay, "A fast and accurate single frequency estimator", *IEEE Transactions on Acoustics, Speech, and Signal Processing*, Vol. 37, No. 12, pp. 1987–1990, Dec. 1989.

[42] M. P. Fitz, "Further results in the fast estimation of a single frequency", *IEEE Transactions on Communications*, Vol. 42, No. 234, pp. 862–864, Feb. 1994.

[43] S. M. Kay, *Fundamentals of Statistical Signal Processing: Estimation Theory.* New York, USA: Prentice-Hall, 2010.

[44] H. V. Poor, *An Introduction to Signal Detection and Estimation*, 2nd ed. New York, USA: Springer-Verlag, 1994.

[45] *Base Station (BS) conformance testing Part 2: Radiated conformance testing (Release 15)*, 3GPP TS 38.141-2 V15.0.0 Standard, available at: https://www.3gpp.org/ftp/Specs/archive/38_series/38.141-2/38141-2-f00.zip

[46] A. Maltsev, *60 GHz WLAN Experimental Investigations*, IEEE Standard 802.11-08/1044r0, Sep. 2008.

[47] Q. C. Li, G. Wu, and T. S. Rappaport, "Channel model for millimeter-wave communications based on geometry statistics", *Proc. IEEE Globecom Workshops (GC Wkshps)*, Austin, USA, pp. 427–432, Dec. 2014.

[48] Q. C. Li et al., "Validation of a geometry-based statistical mmwave channel model using ray-tracing simulation", *Proc. IEEE Veh. Technol. Conf. (VTC)*, Glasgow, U.K., pp. 1–5, May 2015.

Alessio Fascista (S'19) received the Eng. degree in Computer Engineering (summa cum laude) in 2015, and the PhD degree in Engineering of Complex Systems in 2019, both from the University of Salento (Lecce, Italy). In 2018, he was a visiting PhD with the Signal Processing for Communications & Navigation (SPCOMNAV) group, Department of Telecommunications and Systems Engineering, Universitat Autònoma de Barcelona (UAB), Spain. His main research interests are in the field of telecommunications with focus on statistical signal processing for terrestrial localization systems.

Angelo Coluccia (M'13–SM'16) received the PhD degree in Information Engineering in 2011 from the University of Salento (Lecce, Italy). He is currently in tenure-track for Associate Professor at the Department of Engineering, University of Salento, where he teaches the course of Telecommunication Systems. He has been research fellow at Forschungszentrum Telekommunikation Wien (Vienna, Austria), and held a visiting position at the Institut Supérieur de l'Aéronautique et de l'Espace (ISAE-Supaero, Toulouse, France), in the Signal, Communication, Antennas and Navigation Group. His research interests are in the area of multi-sensor and multi-agent statistical signal processing for detection, estimation, learning, and localization problems, with application to radar and wireless networks (including 5G, smart devices, social networks). He is member of the Special Area Team in Signal Processing for Multisensor Systems of EURASIP.

Henk Wymeersch (S'01–M'05) obtained the Ph.D. degree in Electrical Engineering/Applied Sciences in 2005 from Ghent University, Belgium. He is currently a Professor of Communication Systems with the Department of Electrical Engineering at Chalmers University of Technology, Sweden. Prior to joining Chalmers, he was a postdoctoral researcher with the Laboratory for Information and Decision Systems at the Massachusetts Institute of Technology. His current research interests include cooperative systems and intelligent transportation.

Gonzalo Seco-Granados (S'97–M'02–SM'08) received the Ph.D. degree in telecommunications engineering from the Universitat Politecnica de Catalunya, Spain, in 2000, and the M.B.A. degree from the IESE Business School, Spain, in 2002. From 2002 to 2005, he was a member of the European Space Agency, where he was involved in the design of the Galileo System. In 2015, he was a Fulbright Visiting Professor with the University of California at Irvine, CA, USA. Since 2006, he has been with the Department of Telecommunications, Universitat Autònoma de Barcelona, where he has been Vice Dean of the Engineering School since 2011 and he is currently a Professor. His research interests include satellite and terrestrial localization systems. Since 2018, he has been serving as a member of the Sensor Array and Multichannel Technical Committee of the IEEE Signal Processing Society. He was a recipient of the 2013 ICREA Academia Award.